Structural and electronic properties of $(TiO_2)_{10}$ clusters with impurities: A density functional theory investigation

R.H. Aguilera–del–Toro [a,b]

[a] *Departamento de Física Teórica, Atómica y Óptica, Universidad de Valladolid, Spain*

F. Aguilera-Granja [b*]

[b] *Instituto de Física, Universidad Autónoma de San Luis Potosí, San Luis Potosí, México*

E. E. Vogel[c,d]

[c] *Departamento de Ciencias Físicas,*
Universidad de la Frontera, Temuco, Chile and and
[d] *Center for the Development of Nanoscience and*
Nanotechnology (CEDENNA), 9170124 Santiago, Chile

(Dated: February 16, 2019)

Abstract

We report the structural, energetics, and electronic properties of free-standing binary clusters $(TiO_2)_{10}$ with substitutional metallic and non-metallic impurities. The selected $(TiO_2)_{10}$ cluster has tetrahedral symmetry and is the putative low energy structure for this size. The substitutional impurity can be located at a vertex (4 sites) or at an edge (6 sites). The former has a binding energy only 0.03 eV/atom less than the latter, so they can be considered as almost degenerate. A total of 28 impurities are considered in the present report. We study the edge substitutional place since this environment is very similar to the corresponding one in the bulk, which makes these system a model for the bulk-like structures. Another advantage of the cluster considered here is that its energy gap is as large as the one presented in the bulk phases (anatase an rutile). This system allows us to mimic the bulk behavior without the use of intrasite Coulomb corrections (U) usually applied to the $3d$ orbital electrons of Ti atoms U_d and $2p$ orbital electrons of the O atoms U_p; they are generally applied as parameters to fit the real energy gap observed in bulk (TiO_2) systems. We show results for the formation energies, energy gaps and magnetism suggesting a way to control the band gap by means of the use of the appropriate impurity used in the substitution.

I. INTRODUCTION

Titanium oxide in bulk phase and in nanoparticles (NPs) is among the most marketed and used oxides in the materials industry due to the large number of applications in fields as diverse as photo-catalysis, cosmetics, bakery, and so on[1–7] In particular a great effort has been done to improve the photo-chemical activity of (TiO_2) in the anatase phase since it only shows response to the UV light as a consequence of its huge band gap, responding to a very narrow region of solar radiation (less than 5% of the total energy). Some of these attempts try to reduce the band gap by doping the material with metal and non-metal elements.[8–12] To this aim, both theoretical and experimental studies in bulk,[8,9,13] thin films and nano-systems have been carried out to see the benefits obtained with different dopants.[10–12]

In the case of clusters Salazar-Villanueva and coworkers studied $(TiO_2)_n$ for selected sizes $n = 10$ and $n = 19$ introducing semi-conductor impurities like C, Si, Ge, Sn, Zn, Ga and Ge.[10,11] On the other hand, bulk systems in both the anatase and rutile phases have been studied with the presence of conducting metallic impurities; in particular $3d$ Transition Metals (TM) and some selected $4d$ TM (such as Mo) and very few of the $5d$ series (such as as Os and Pt) have been reported.[8,9,14–16]

In general, the results for clusters and bulk systems indicate that the gap slightly decreases when non-metallic impurities are used; for metal impurities more complex dependencies are observed.[10,11,17,18] In the case for bulk-like systems most of the calculations are done for $3d$-TM dopants where early calculations were done for the paramagnetic regime[8,9]; one finding was that the position of the impurity levels shifted to lower energy values as the atomic number of the TM increased. However, these results are limited and could be even inadequate for TM-impurities where magnetic interactions need to be included. More recent calculations have considered magnetic interactions in the case of TM-impurities studies getting more reliable results.[14–16,19] Moreover, recent studies have shown that even in the case of non-magnetic impurities (like carbon) the calculations have to be done in a spin-polarization framework to properly describe the behavior of the system.[20]

In the case of bulk (TiO_2), DFT studies tend to underestimate the energy gap leading to about a half of the value experimentally measured for the pure system (Eg=3.23 eV), as it can be seen in the work by S.G. Park[21] and reference therein. The previous underestimation in the band gap can be corrected using hybrid functionals or adjustments in the Hubbard intra-

sites interaction U in the Ti and O orbitals by means of GGA+U or LDA+U.[21–23] Therefore to perform a reliable study for TM-impurities in the bulk phase we must first correct the gap, and later on dope the system including the magnetic interactions by performing a polarized spin calculation.[24,25]

In this work we consider the recently reported tetrahedral cluster of $(TiO_2)_{10}$ as a basic structure for the study of (TiO_2) bulk with impurities.[26,27] One important advantage of using this tetrahedral cluster is that it does not need intrasite interactions to present a band gap comparable to those of anatase (3.23 eV) and rutile (3.02 eV) in their bulk phases. This work is on the line of ancient calculations that used fragments of the real system to perform volumetric studies.[28] Thus, the basic cluster used in this work is representative of anatase and rutile in a natural way. Therefore, it can be used as a building block to mimic the titaniun dioxide bulk systems. This work begins with a thorough study of several physical properties of 28 different substitutional impurities in $(TiO_2)_{10}$ (also $(TiO_2)_{20}$ for some specific comparisons). Rather that pointing to obtain exact numerical values for each impurities the emphasis is on the general tendencies present for each family of dopants which can be exported from small clusters to bulk systems.

II. THEORETICAL APPROACH AND COMPUTATIONAL DETAILS

Our calculations are based on Density Functional Theory (DFT) within the generalized gradient approximation (GGA) formulated by Perdew-Burke-Ernzerhof (PBE),[29] as implemented in the computational package SIESTA (Spanish Initiative for Electronic Simulations with Thousands of Atoms).[30] SIESTA employs numerical pseudo-atomic orbitals as basis sets to solve the single particle Kohn-Sham equations, while the atomic cores are described by nonlocal norm-conserving Troullier-Martins pseudopotential[31] factorized in the Kleinman-Bylander form.[32] The pseudo-potentials for Ti and O, were generated using the valence configurations $4s^2 3p^6 3d^2$ and $2s^2 2p^4$, respectively. The s, p and d cut-off radii for Ti are all equal to 1.98 a.u., and the s and p radii for O share the value 1.14 a.u.. The valence states were described using double-ζ doubly polarized basis sets. Further details about the pseudopotentials and basis sets used for the impurities, as well as about the pertinent tests, can be found in our previous works.[33,34]

All the cluster calculations were performed using a cubic box ($20\mathring{A} \times 20\mathring{A} \times 20\mathring{A}$) large

enough such that interactions between the cluster and its replicas in neighboring cells are negligible. For instance, the shortest distances among the different images is of approximately 13 Å. We have made several proofs to confirm the independence of the total energy values obtained in our calculations for different box sizes. Only the Γ-point was used for the Brillouin zone integration. We used energy cutoff of 250 Ry to define the real-space grid for the electron density. For the geometric optimization of the atomic structures, we employed the conjugate gradient method[35] as implemented in SIESTA until the interatomic forces were smaller than 0.006 eV/Å. We perform full spin polarization calculations and full relaxation without any constrains in the optimization.

A. Atomic configurations

Most of the present work is based on a particular $(TiO_2)_{10}$ cluster, which presents tetrahedral symmetry and has proven to be the most stable geometrical structure for a TiO_2 cluster so far, it is worth noticing this cluster presents an energy gap comparable to the bulk gap (3.31 eV).[26] There are two possible sites as candidates for admitting a substitutional impurity: at the vertices and at the edges of the $(TiO_2)_{10}$ tetrahedron. Both sites offer low energy conditions in comparison with any interstitial inclusion of impurities. In general, the most favorable site for a substitutional impurity is the vertex. However, for most of the impurities the energy differences with respect to the edge site is less than 0.03 eV/atom, which makes these two configurations as almost degenerate even at zero temperature which is the case in the present study. Coordination number at a vertex are very seldom in the bulk, while conditions at an edge site are more similar to what substitutional impurities will find on the surface of materials. Since in this work we want to stay close to systems that mimic the bulk behavior we will focus on impurities occupying the edge sites. In such cases the local coordinations of Ti-atoms is related to the six-fold coordinated sites in both rutile and anatase phases, where six oxygens occupy positions as first nearest neighbors. In addition the $(TiO_2)_{10}$ cluster presents 4 vertex positions and 6 edge positions as shown in Fig. 1 a) and b); so in equal energy conditions it is an edge position the most likely one, which we can extend to the nearly degenerate case to some extent.

Another advantage of using this finite cluster as a model for bulk behavior is that it reproduces the main characteristics of the density of states of the bulk concerning the type

of energy levels and even the energy gap.[26] This last point is very important since a finite size bulk calculation (atomic base plus periodic boundary conditions) aiming to produce the appropriate energy gap would need approximations that would imply hybrid functionals or adjustments in the intra-sites interaction U by means of extra terms GGA+U or LDA+U, as already mentioned above but here we discuss it more broadly.[21–25] These corrections to the Coulomb contribution (U) are applied to the $3d$ orbital electrons of Ti atoms U_d and $2p$ orbital electrons of the O atoms U_p as adjustable parameters to fit the energy gap close to the values observed in bulk (TiO_2) systems. Empirical rules for using parameters U_d and U_p can be seen in Parks' work,[21] where it is shown how the gap can be adjusted as much as desired. This fit has two disadvantages: on one hand it introduces energy terms difficult to interpret in reality, while on the other hand it implies costly computer calculations. We propose to avoid all of this by using a cluster which from the very start posseses a band gap and density of states similar to the bulk system without the introduction of fitting parameters.

III. RESULTS

In Fig. 1(a) and (b) we present two different views of the geometrical structure of the $(TiO_2)_{10}$ cluster considered here: light gray balls represent Ti atoms, small red balls are Oxigen atoms and a green ball represents an impurity on one of the 6 edge positions. Fig. 1(c) highlights the environment of the substitutional impurity in the $(TiO_2)_{10}$ cluster. For comparison, Fig. 1(d) shows the environment of the substitutional substitutional impurity for the rutile phase.

The optimized geometrical structure after relaxation shows small deformations that depend on the impurity. In general, for the case of the sp elements the local symmetry is broken and the impurity is displaced towards one of the Ti atoms (depending on the valence of the impurity). These new positions tend to open the two faces of the tetrahedron not connected to the impurity in a way that resembles the wings of a flying butterfly; this effect is more pronounced for the light elements. Exceptions are Al and Si whose presence leaves the pure cluster structure basically unaltered. In the cases of impurities involving the $3d$ and $4d$ TM the tetrahedral geometric structure is only slightly altered and only small deformations modulated by the atomic radius sizes are presented; this effect is also observed for

the middle and late $5d$.

The density of states (DOS) of the $(TiO_2)_{10}$ pure system (putative Ground State (GS) structure) is presented in Fig.2. The occupied electronic levels are marked by horizonatal lines under the curve while the energies of the empty states are left unmarked. The system presents a clear insulator behavior with a band gap of 3.31 eV, which has already identified as very close to the energy gaps for the anatase and rutile bulk phases. The gap was calculated by means of the HOMO and LUMO states. As the different dopants are considered the values of the HOMO and LUMO energies change accordingly, however it is important to use the DOS given in Fig. 2 for the pure system as a reference when discussing the electronic properties of the doped structures.

The binding energy E_b of the altered system Ti_9XO_{20} (X is a specific impurity for each system), defined as the total energy per atom, is obtained in the following way:

$$E_b[(Ti_9XO_{20})] = \frac{E_{Total}[(Ti_9XO_{20})] - 9E_{atom}(Ti) - E_{atom}(X) - 20E_{atom}(O)}{30} . \quad (1)$$

Once the binding energy converges according to the protocol described in previous Section the structure is accepted as stable. The binding energy (in eV/atom) is illustrated in Fig. 3 using the atomic number of the impurity as the abscissa.

It is interesting to notice that the variation of binding energy values for this set of 29 systems are contained in a range of about half eV per atom only and all of them lay near or under -7.0 $eV/atom$. Actually the most stable structure remains the pure system for Z=22. In general the binding energy stability decreases almost in a monotonic way as a function of the atomic number within each series; exceptions are observed for Si, Cr and Mn and some inflections for the $4d$ and $5d$ series.

If we use the pure system as a reference we can say that the variations in the binding energy are always positive and in the range of 0.08 and 0.5 eV/atom. The smallest differences appear at the beginning of the series increasing from there with the atomic number.

The formation energy is defined as:

$$E_{Formation}[(Ti_9XO_{20})] = E_{Total}[(Ti_9XO_{20})] - E_{Unrelaxed}[(Ti_9O_{20})] - E_{atom}(X). \quad (2)$$

Results for this function are presented as open circles in Fig. 4 using the atomic number as the abscissa. For comparison the previously discussed binding energy results are superposed here as small filled circles; the different scale for these two different energies is apparent.

7
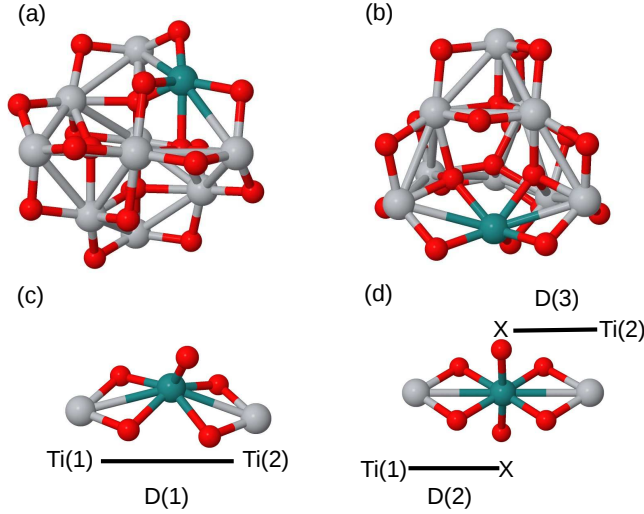
FIG. 1. (Color online) In (a) and (b) two views of the cluster $(TiO_2)_{10}$ used in most of the present calculation. Oxygen atoms are represented by small (red) balls, Ti atoms are represented by clear large balls; the edge site to be occupied by the impurity is marked in darker color. The local environment surrounding the impurity in the cluster is shown in (c). The equivalent environment for the bulk rutile phase is shown in (d). Distances $D(1)$, $D(2)$ and $D(3)$ are used in Eq. (3).

The ordering in the series is similar to the one observed for the binding energy per atom with Si, Cr and Mn altering the monotonic dependence with the atomic number. Inflections points are again present for the $4d$ and $5d$ series.

Results for the geometrical properties of the clusters Ti_9XO_{20} are presented in Table I, separated by series according to the electronic labeling. In first column we list the impurities (and its atomic number in parenthesis). The second column gives the number of oxygen neighbors to the X-impurity in the structure. Twin columns three and four give the two different Ti-X distances on the same edge (the impurity is usually displaced from the central position). Column five gives the average Ti-X distance obtained from the values in previous columns. Column six renders the value for the deformations parameter D as defined by Eq. (3) in terms of the distances shown in the Fig. 1:

$$D = \frac{D(1)}{D(2) + D(3)} ,$$
(3)

where $D(1)$ is the direct distance between the two Ti atoms on the edge where the impurity is placed, while $D(2)$ and $D(3)$ are the distances between the X-impurity and the Ti atoms

8
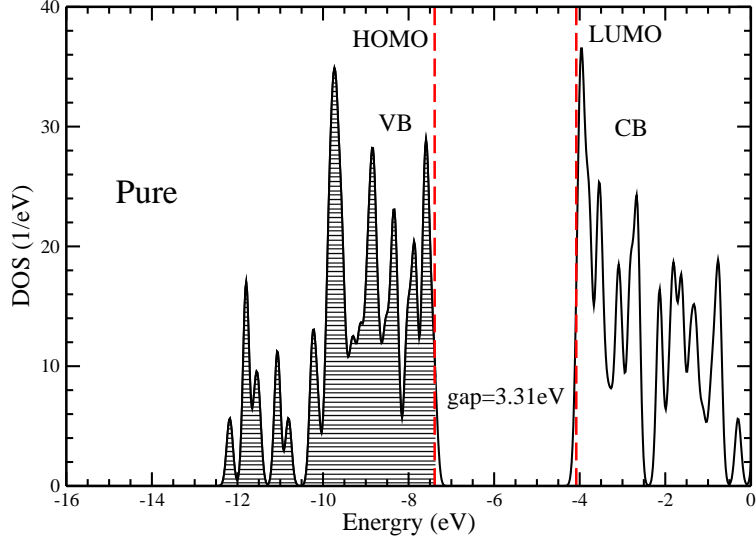
FIG. 2. (Color online) Ground state DOS for the cluster $(TiO_2)_{10}$ to be used as a reference for the DOS in the presence of impurities. The dashed vertical lines mark the gap of the system considering the eigenvalues of the problem. Horizontal lines indicate the occupied states. VB (CB) stands for Valence (Conducting) Band.

on that edge. For example in the case of F(W) the direct distance $D(1)$ is 6.382 (5.548) Å, $D(2)$ and $D(3)$ are 3.820 (2.980) and 6.090 (3.010) Å, respectively, then the deformation parameter is $D = 0.644$ (0.952) which corresponds to the largest (lowest) deformation for the system included in Table I.

In Fig. 5 we present the interatomic X-O average distances, which present a grouping according to the electronic properties of the series but the dependence with the atomic number is non monotonic. The group $2sp$ presents the shortest X-O distances, with X=N as the true minimum. The $3sp$ series presents a larger distribution of distances with X=P at the minimum. The $3d$ family presents a cloud of distances just underneath the average distance for the undoped system, which is marked by a horizontal dashed line. Both $4d$ and $5d$ families present clouds with values just over the distance for the undoped system. Worth noticing, the X-O average distances for Al and Si are comparable to the $3d$ cloud, which is in agreement with the oxygen coordination number as presented in column two of Table I. The nobel metals tend to present large X-O distances, which is clearly appreciated for the cases of Au and Ag presenting the largest distances in Fig. 5. In the $3d$ series the Cu-O distance is large but not large enough and it is the third of the family just under the distance for Cr-O.

9
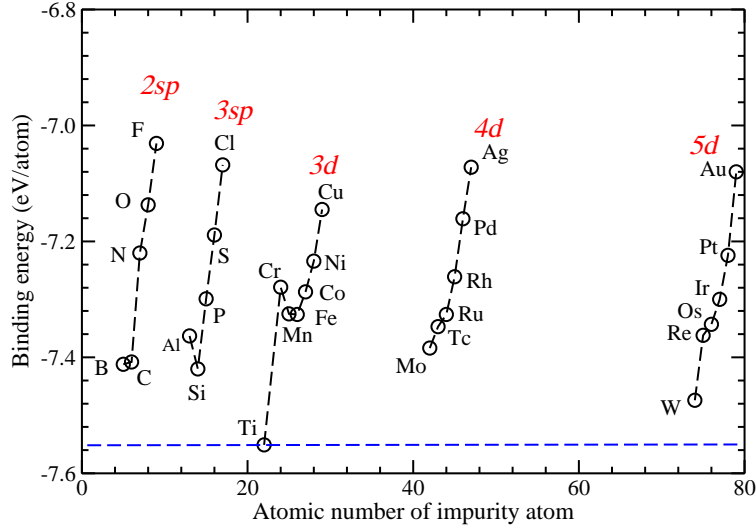
FIG. 3. (Color online) Binding energy for the Ti_9XO_{20} system doped with the different impurities. The horizontal dashed line corresponds to the undoped system (Ti as a fake impurity) to be used as a reference.
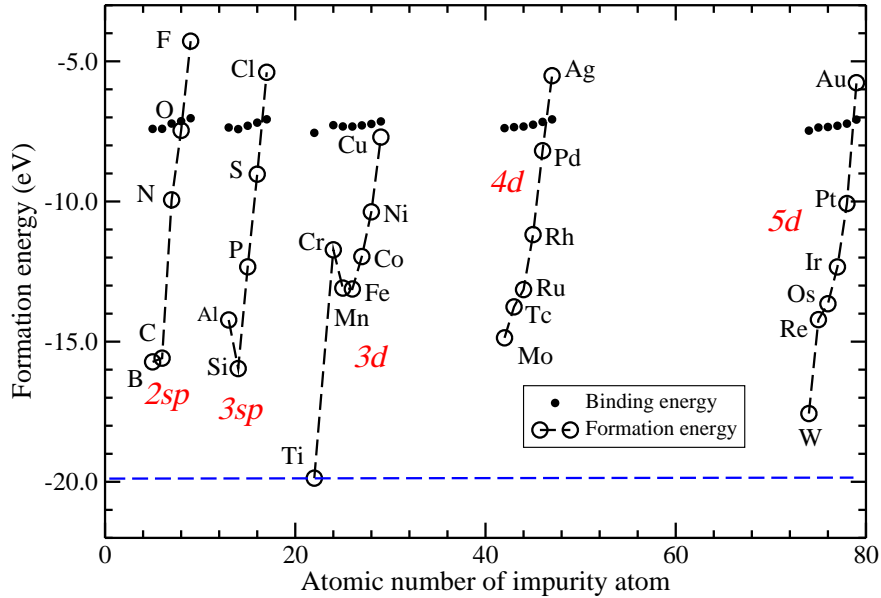
FIG. 4. (Color online) Formation energy (open circles) for the Ti_9XO_{20} system with the different impurities. Additionally, previously reported binding energies are also included here by means of small filled circles. The horizontal dashed line corresponds the pure case.

The dependence of the average Ti-X distance on the impurity is shown in Fig. 6. In the case of the $2sp$ series this distance increases monotonically with the atomic number; when going from B to O it varies from 2.85 to 2.95 $\mathring{A}$, reaching an average value of almost $5\mathring{A}$ for

10
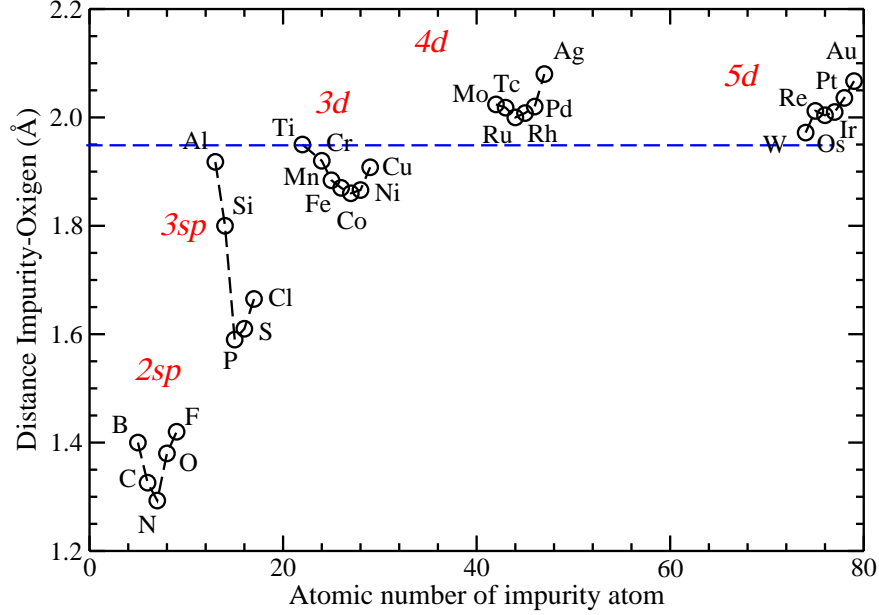
FIG. 5. (Color online) Interatomic distance X-O for the Ti_9XO_{20} systems for the different impurities. The horizontal dashed line corresponds to the Ti-O distance to be used as a reference.

the case of F. The series of $3sp$ presents a Ti-X average distance increasing with the atomic number with the only exception of Si. In the case of the $3d$ series the distances fall in a cloud with values just under the value for the undoped cluster that is indicated by a horizontal dashed line. Both $4d$ and $5d$ series present clouds with values just over the undoped system with a small deviation for the case of Ir.

The deformation parameter presented in column six of Table I deserves a special discussion. The case of F is by far the one that deforms the most the original structure due to its large electronegativity. From this argument it is not surprising that the next impurities deforming the original system are Cl, O, P and S all of them accompanying F in the upper right corner of the periodic table. On the contrary, the impurities that almost pass unnoticed in deforming the original cluster are Cr, Mo y W which are isoelectronic among them and occupy the fourth column of the transition metal elements. Other d systems deviate only slightly from the reference value 0.957 corresponding to Ti in Table I. Due to the similar environment it can be expected that the general trends presented by our results of valid for small clusters (Table I) are also valid for bulk when the deformation parameter is close to the reference value (undoped case).

The magnetic moments for all the clusters are presented in Fig.7 with open circles, the local magnetic moments for the corresponding impurity are presented by means of small

11
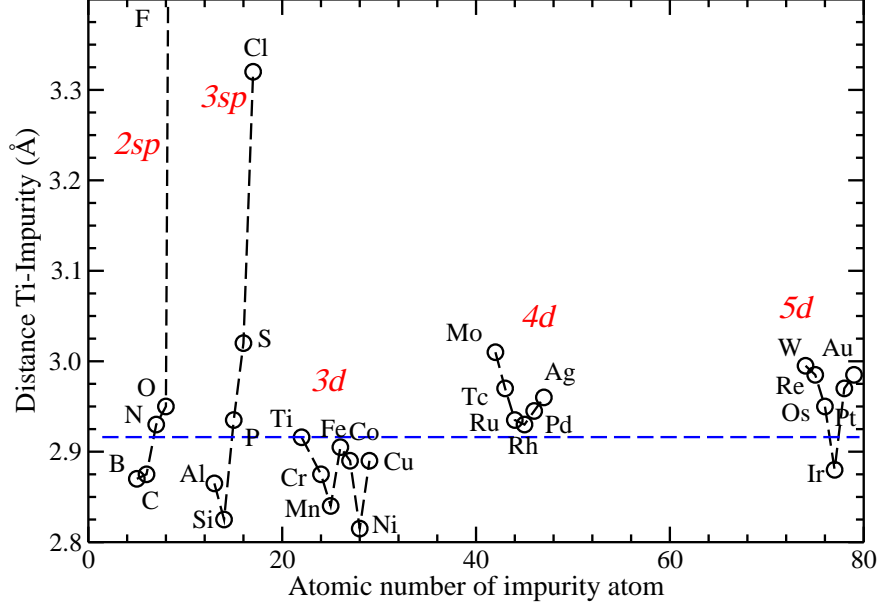
FIG. 6. (Color online) Interatomic distance Ti-X for the Ti_9XO_{20} systems for the different impurities. The horizontal dashed line corresponds to the Ti-Ti distance in the pure system to be used as a reference. The value for F is out of scale (almost 5 $\mathring{A}$).

filled circle. In general, the impurity is coupled to the TiO_2 matrix in a ferromagnetic way, with the exceptions of O for the *sp*-elements and Cr for the TM, both showing antiferromagnetic coupling. Doping with *sp*-elements produce clusters with succesive even-odd magnetic behavior according to the atomic number of the impurity, that is non magnetic for even and magnetic moment of $1\mu_B$ for the impurities with odd number of electrons. The main magnetization for these systems comes from the oxygen atoms as can be seen on the left-hand side of Fig. 7. The magnetization of the TM-impurities have a less monotonous dependence as illustrated in the same figure; here the main source for the magnetic contributions comes from the TM-impurity, which also explains the amplitude reached by the magnetic moment of the system for some impurities. Chromium is anomalous in the 3*d* series presented in Fig. 7, since it presents antiferromagnetic coupling to the matrix. Notice that the total magnetic moment of the system tend to be the same for TM impurities belonging to the same column of the Periodic Table, with with the exceptions of Fe and Co (hard magnetic impurities). The corresponding iso-electronic impurities for Fe (Ru, Os) and Co (Rh, Ir) show different values for the total magnetic moments. There are few reports in the literature on the magnetic properties of impurities in TiO2, however our results agree with those reported for Mo, Os in volume[14,15] and Pt in the case of clusters.[16]

12
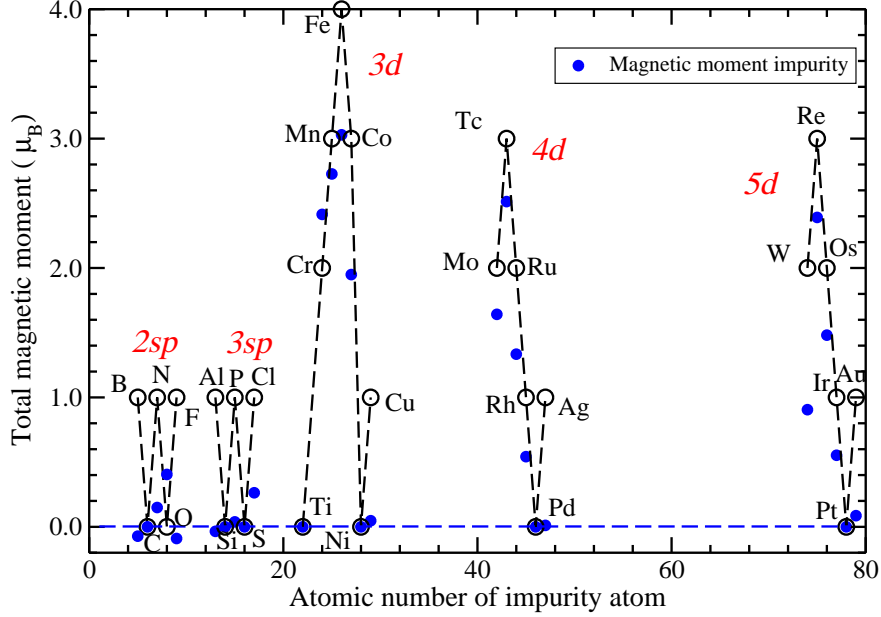
FIG. 7. (Color online) Total magnetic moment for the cluster Ti_9XO_{20} indicating the impurities by open symbols. In the cases of Fe, Co and Ni additional calculations with fix-spin value were carried out to be sure that the magnetic solution is the right one. Small filled symbols show the local magnetic moment of the impurities.

The cluster $(TiO_2)_{10}$ is almost a non-polar material, that is, its electric dipole moment is practically zero (0.021 Dbys). However, the inclusion of a different element in the matrix produces a redistribution of charge, which can lead to an electric dipole in the system. In Fig. 8 we present the charge transferred from the impurity to the matrix. The dashed line in this figure represents the value for the case of the undoped cluster. All those impurities close to this horizontal line lead to an electric polarity equivalent to non-polar systems. The elements that are more distant from this reference line in each series (F,S, Cu, Ag and Au) produce the systems with the largest electric dipoles as can be seen also in Fig. 9. In this same figure, it is illustrated how the electric dipole grows monotonically with the atomic number for the $2sp$ series. However, for the other series a zig-zag behavior prevails leaving at the middle of the series the impurities leading to the lower electric dipole of the respective set (P, Mn, Ru and Os).

The most important magnitude to be monitored along the impurity variations is the energy gap of each doped cluster. The reference value is the undoped cluster whose gap is
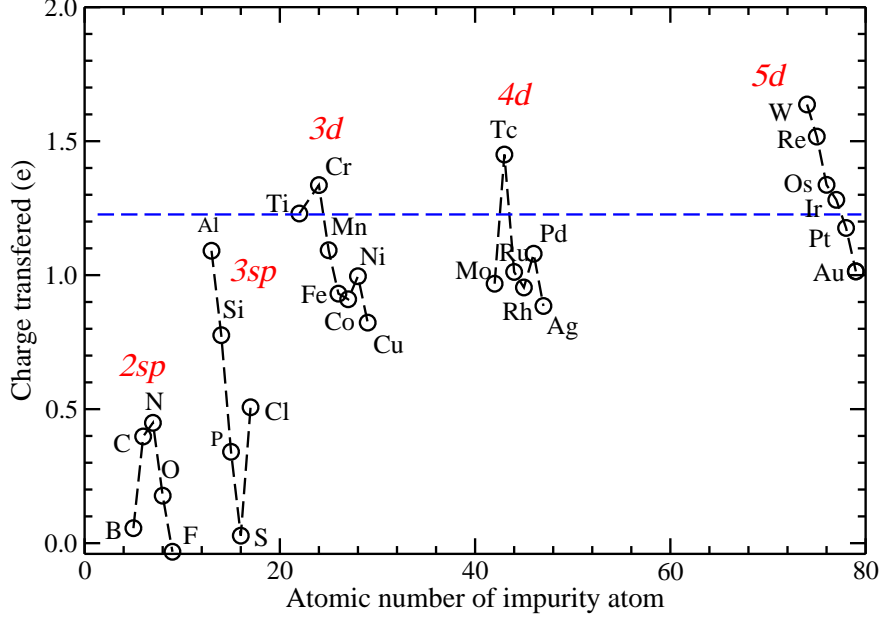
FIG. 8. (Color online) Charge transferred from the impurity to the matrix in the cluster Ti_9XO_{20}. The positive value indicates that the matrix lost electrons. Notice that F is the only one gaining electrons although in a marginal way. The horizontal dashed line corresponds to the pure system.

3.31 eV (very similar to the bulk values in rutile and anatase). Fig. 10 shows the energy gaps for doped systems according the atomic number of the impurity. The horizontal dashed line is a reference for the undoped material where Ti is a fake impurity to complete the series.

The first general result is that the gap is extremely sensitive to the type of impurity placed at the edge position. Thus, substituting atoms from the $2sp$ group narrows the gap to a few tenths of eV with the exceptions of C and N: the former keeps the system as an insulator introducing states under the VB, while the latter turns the system into a semimetal or narrow gap semi-conductor with states near the bottom of CB. For the $3sp$ series, Si and S have a behavior similar to C only closing the gap a bit more while P follows the tendency of N in the previous series. The cases of Al and Cl is similar to the cases of B and F atoms.

TM impurities offer a variety of possible gaps ranging from 1.41 eV in the case of Tc to 0.17 for W. So upon choosing the right TM substituting element the energy gap can be tuned between a normal semiconductor to a narrow gap semiconductor with a gradual distribution of possible energy gaps. The choice of the right impurity for a given purpose can be combined with other desired properties of the system.

A very important condition is the position of the Fermi level E_F for the case of each

14
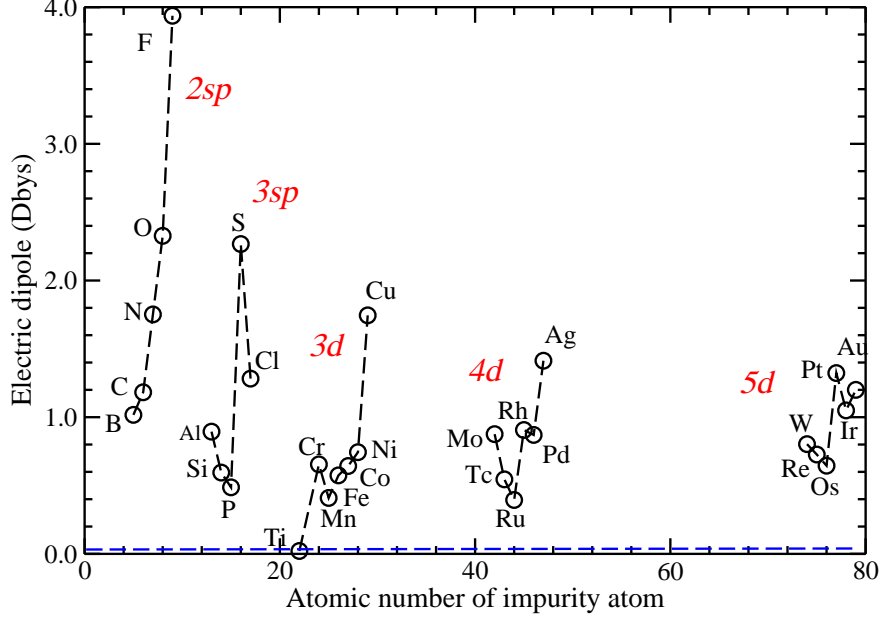
FIG. 9. (Color online) Total electric dipole as a function of the different impurities for the Ti_9XO_{20} system. The horizontal dashed line corresponds to the pure system.

dopant. These results are presented as circles in Fig. 11, which indirectly tells us the position of the energy levels of the impurity without looking into each density of states. In addition we have also included here as dashed lines the HOMO and LUMO values of the pure system to be used as references. However, it is important to bear in mind that the presence of the impurity may slightly alter these values. The energy gap ranges are given by the color of the circle as indicated by the inset of Fig. 11.

We now discuss the different series as presented in Fig. 11. For the $2sp$ ($3sp$) group E_F is closer to the HOMO as comperared to the pure system with the exception of N (P) which is closer to LUMO; the impurity levels are closer to the VB and/or CB. Occasionally, some impurity present deep levels like in the case of C (Si). The gap ranges from intermediate to large with the exception of the gap of N (P) which is small.

In the case of the $3d$ group (from Cr to Cu) E_F is found in a small region near HOMO progressing towards VB in a non monotonic way; the impurity levels lay in between VB and CB originating both small and large gaps. Cr is particularly interesting since its level lay just in the middle producing and intermediate gap.

E_F descents almost monotonically with the atomic number for the $4d$ ($5d$) series, presenting a "shoulder" for the case of Ru (Os very slightly). In the case of the $4d$ series The impurity levels are in between CB and VB slightly closer to the latter, giving rise to small

15

gaps since E_F is surrounded by impurity levels. Exceptions to this behavior are Tc and Pd: the former produces a large gap since E_F is over the impurity levels; the latter produces an intermediate gap due to the spread of the impurity levels which is larger to any other element of the series. In the case of the series $5d$ the impurity levels are in between the bands descending monotonically from near CB to near VB as the atomic number increases showing a great dispersion. Since the E_F is surrounded by impurity levels intermediate gaps are produced, with the exceptions of the small gap of W (E_F is over its impurity levels and near CB) and the large gap of Pt (its impurity levels split laying either close to VB or CB).

The spin polarized DOS of Ti_9XO_{20} for the elements of the series $4d$ are presented in Figs. 12 and 13. The position of the HOMO and LUMO were obtained from the corresponding eigenvalues. For the representation of the DOS we have used a broadening of 0.1 eV, which is the reason for the tails above (HOMO) and below (LUMO). The dashed lines (under the DOS graphic) indicates the occupied states. The VB is at the left of the HOMO (H), while the CB is at the right of the LUMO (L). Starting with Mo (top) the impurity states are in the vicinity of the CB, going to Tc (middle) the states of the impurity go towards the proximity of VB, them, continuing to Ru at the end (botton) the impurity levels are found again towards the center of the band gap. The analysis continues in Fig. 13 with Rh (top) where the impurity levels are scattered throughout the gap. As we continue to Pd (middle) and Ag (bottom) we find the impurity levels closer to VB.

Previous results and discussions show in general that a variety of positions for the impurity levels within the gap are found; this is particularly true for the $2sp$, $3sp$ and $3d$ series. Moreover, such positions do not follow any monotonous order with respect to the atomic number as the one presented by the Fermi level in the cases of the $4d$ and the $5d$ series as illustrated clearly in Fig. 11. So no a priori behavior can be ventured in general previous to the calculations.

A.   Size effects and comparison

It has been pointed out by Umebayashi[8] that in the case of $3d$ transition metals doped in (TiO_2) rutile, the localized levels shifts to lower energies as the atomic number of the dopant increases. In spite this work does not consider magnetism in the calculation these general results serve as a general reference for related contributions like ours. Actually, this

observation is in agreement with our model but only in the paramagnetic case (non polarized calculations) as it can be seen from the position of the Fermi level. Thus, for Cr, Mn, Fe, Co and Ni our results for the E_F are -4.97 eV (gap aprox 0.59eV), -5.22 eV (mini-gap aprox 0.22eV), -5.75 eV (mini gap 0.12eV), -6.23 eV (gap 0.87 eV) and -6.39 eV (gap 0.59 eV) respectively. As it can be appreciated the E_F tends to lower energies as the atomic number of the impurity increases.

As it can be noticed the impurity concentration is 10 % for the case of our $(TiO_2)_{10}$ cluster without the possibility of reaching lower concentrations. To overcome the difficulty of the high impurity concentration we consider (for this purpose only) the larger cluster $(TiO_2)_{20}$ which has also tetrahedral structure and an energy gap (3.22 eV) very close to the one of $(TiO_2)_{10}$ cluster and also close to the gap of the bulk in pure system. This tetrahedral structure is the putative ground state for $(TiO_2)_{20}$ as demonstrated by F. Illas and coworkers.[27] For an edge impurity in the twice as large cluster (5 % concentration) in the case of the paramagnetic regime we get the following Fermi levels: -5.57 (gap= 0.58eV), -5.81 (gap= 0.29eV), -6.27 (mini gap=0.15 eV), -6.89 (gap=0.88 eV) and -7.05 (gap=0.68 eV) for Cr, Mn, Fe,Co and Ni impurities respectively. As it can be seen these results (valid for the paramagnetic case) are only slightly different from those of the smaller cluster and higher concentration (quoted in the previous paragraph). These combined results favor the idea of approaching the bulk behavior with clusters that mimic the main features of the bulk.

Nevertheless, when the spin polarization is considered the dependence of the energy levels with the atomic number is far from lineal as commented in the previous two paragraphs for the paramagnetic case. This is evident from the results presented in Fig. 10 which show that this is evan more so for the impurities with strong magnetic character such as the 3d-TM. As a way to rule out a determinant size dependence we did the same calculations (spin polarized) for the larger cluster, namely $(TiO_2)_{20}$ finding results similar to those of the small cluster used in most of this paper. As an example we list next the comparative results for the 3d series ordered as Cr, Mn, Fe, Co, Ni and Cu. In the case of $(TiO_2)_{10}$ we get the following ordered E_F values (and corresponding gaps) -5.96 eV (gap 0.84 eV), -5.62 (gap 1.27 eV), -6.19 (gap 1.11 eV), -6.20 (gap 0.40 eV), -6.40 (gap 0.58) , and -6.84 (gap 0.51 eV) respectively (open circles in Fig. 10). The equivalent results for $(TiO_2)_{20}$ are -6.47 eV (gap 0.92 eV), -6.42 (gap 1.40 eV), -6.64 (gap 1.54 eV), -6.63 (gap 0.13 eV), -7.05 (gap

0.69), and -7.29 (gap 0.63 eV) respectively (small close circles in Fig. 10). The values for the energy gap follow the same tendency for both clusters; The Fermi level values are a bit more negative in the larger cluster (15 % at the most) but without changing the behavior observed in the smaller one. These results are important to indicate that the calculations performed with TM impurities in $(TiO_2)_{10}$ have the basic ingredients to mimic the general properties of the bulk (TiO_2) with impurities.

Finally, our results for the band gap follow the same behavior as those reported by Y. Wang and coworkers[13] using PBE[29] within the GGA approximation. What the cited work reports are the HOMO-LUMO values with respect to the impurity levels (which is unusual since most of other works use VB and CB of the doped system as reference levels). In any case Wang's results for the HOMO-LUMO (using the VB and the CB as references) are 0.92 eV for Cr, 1.68 eV for Mn, 0.69 eV for Fe, 0.51 eV for Co, 0.23 eV for Ni, and 0.63 eV for Cu, while ours are 0.84 eV, 1.27 eV, 1.11 eV, 0.40 eV, 0.58 eV, and 0.51 eV, following the same sequence. The differences in the values can be due to the fact that Wang's calculations are intended for the anatase phase, and in their calculations the bulk band gap is underestimated (they obtain 2.21 eV instead of 3.2 eV which is the actual value). As presented above, our calculations are more adequate to represent (actually mimic) the rutile phase and strictly corresponds to finite size (cluster with impurities). It is important to underline again that previous results are clearly different from those obtained in the paramagnetic approximation,[8,9] thus showing the importance of performing spin-polarized calculations.

IV. CONCLUSIONS

The simulated results for edge substitutional impurities in $(TiO_2)_{10}$ in all cases and in $(TiO_2)_{20}$ for some selected cases allow us to give general tendencies of the role of such impurities in TiO_2 in the bulk and in the rutile phase in particular. This is so because these two clusters retain most of the electronic properties of the bulk which makes them good candidates to test the system at a smaller scale. In particular, the energy gap of the clusters is very close to the corresponding one in rutile (see Fig. 2).

The binding energy of the doped $(TiO_2)_{10}$ cluster in general increases as the atomic number of the impurity (See Fig. 3), becoming less stable than the undoped system particularly

at the end of the series, the smallest deviation in energy is presented by W, and largest ones by F, Cl, Ag and Au. The formation energy follows a similar behavior but in a much wider region of energy values (See Fig. 4). The shortest interatomic distances between the impurity and the oxygen atoms are observed for the non-metallic impurities; TM-O distances are slightly different from those of the pure system. The impurities deform the local environment presenting the greatest deformations in the case of non-metallic impurities particularly by F, Cl and S (See Figs. 5 and 6).

The magnetic moment of the Ti_9XO_{20} clusters is mainly given by impurity (X). Generally, the interaction TM-matrix is ferromagnetic with the only exception presented by Cr where the interaction is antiferromagnetic. The non-metallic impurities do not present a significant magnetization; an alternating even/odd behavior in the total magnetization is presented here (See Fig. 7). The charge transfer and the electric dipole show a complex dependence with the atomic number of the impurity; the largest values of both properties are observed for the non-metallic impurities in general (See Fig 8 and 9). Substitutions impurity doping provides a broad range of possible energy gaps with gradual intermediate possibilities; it is then possible to tune to a desired energy gap by choosing the appropriate impurity (See Fig. 10). Naturally, the impurity presence also modifies the Fermi level in a complex way particularly in the non-metallic and the $3d$ impurities; in the cases of $4d$ and $5d$ impurities an almost linear dependence with the atomic number is observed (See Fig. 11).

The modification of the impurity concentration reached by the consideration of the larger tetrahedral cluster $(TiO_2)_{20}$ did not modified the main conclusions obtained from the smaller cluster (See Fig. 10). The main reasons for this being the fact that the geometric structure in both clusters is tetrahedral and that the DOS are very similar with almost identical gaps. The density of states seems to be one of the most sensitive properties affected by doping in the TiO_2 systems and no clear tendency with the atomic number in the impurity states introduced in the gap of the DOS for the TM was found (See Figs. 12 and 13).

Although previous results do not necessarily represent the true values for the corresponding properties in the bulk, they give general tendencies of the range of variations these values could have. In addition, they also provide a guide as to which impurity could be tried in a real TiO_2 system to achieve a desired property.
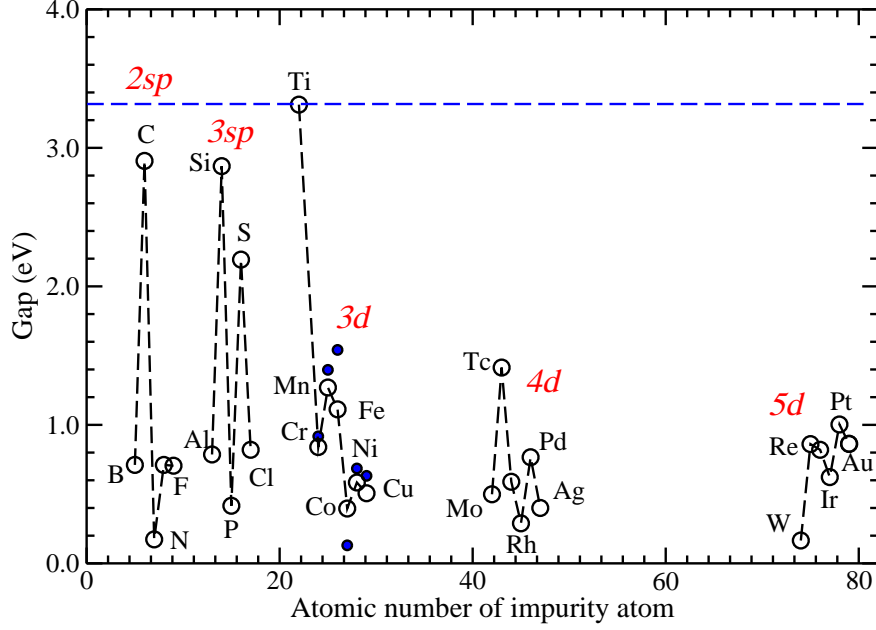
FIG. 10. (Color online) Gap as a function of the different impurities for the Ti_9XO_{20} system; the corresponding eigenvalues were used directly in this calculation. Notice the heart rate shape for the results of the nd-TM series. The gaps calculated for the system $Ti_{19}XO_{40}$ are given by small filled symbols; this twice as large tetrahedral cluster has similar energy gap as the Ti_9XO_{20} system. The horizontal line corresponds to the pure system.

---

* faustino@ifisica.uaslp.mx

FIG. 11. (Color online) Fermi level position as a function of the different impurities for the Ti_9XO_{20} system. Horizontal dashed lines correspond to the HOMO and the LUMO for the pure case as a reference. Open circles correspond to gaps in the range 0.6 to 1.0 eV, grey circles correspond to gaps lower than 0.6 eV, and dashed symbols correspond to gaps larger than 1.0 eV.

[1] T. Daimon, T. Hirakawa, M. Kitazawa, J. Suetake and Y. Nosaka, Applied Catalysis A. General, **340** (2008) 169-175.

[2] G. Rajakumar, A. Rahuman, S. Roopan *et al.*, Spectrochim. Acta, Part A**91** (2012) 23-29.

[3] S. T. Khan, A. A. Al-Khedhairy, and J. Musarrat, J. Nanopart. Res. **17** (2015) 276, (p16).

[4] O. Carp, C. Huisman, and A. Reller, Solid State Chem. **32** (2004) 33-177.

[5] P. V. Kamat, J. Phys. Chem. C **116** (2012) 11849-11851.

[6] M. Chen, T. P. Straatsma, and D. A. Dixon, J. Phys. Chem. A **119** (2015) 11406-11421.

[7] F. Piccinno, F. Gottschalk, S. Seeger, and B. Nowack, J. Nanopart. Res. **14** (2012) 1109-1120.

[8] T. Umebayashi, T. Yamaki, H. Itoh, and K. Asai, Jour. of Phys. and Chem. of Solids, **63** (2002) 1909-1920.

[9] H. Xing Gang, H. Mei Dong, W. Xiao Ling, L. An Dong, Sci China Ser. G-Phys Mech. Astron. **52** (2009) 838-842.
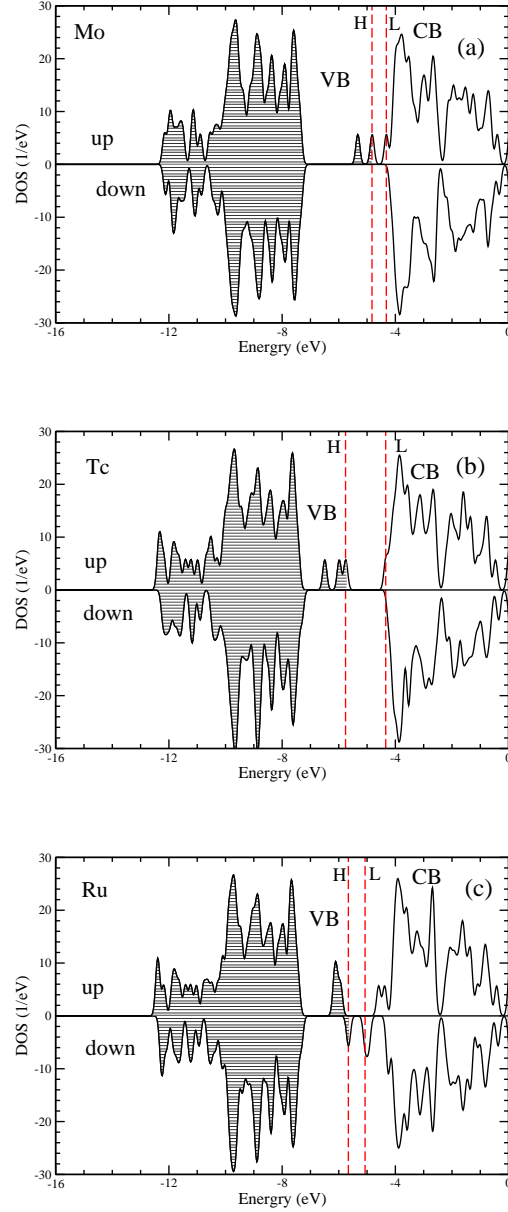
FIG. 12. (Color online) Spin-up and spin-down DOS for Mo (a), Tc(b) and Ru (c) impurities in the Ti_9XO_{20} system (initial part of the $4d$ series). The non-monotonous dependence of the impurity levels can be readily appreciated. Vertical lines correspond to the HOMO (H) and LUMO (L) levels. Horizontal lines mark the occupied electronic states.

[10] M. Salazar-Villanueva, A. Bautista Hernandez, E. Chigo Anota, S. Valdez, and O. Vázquez Cuchillo, Physica E **65** (2015) 120-124.

[11] M. Salazar-Villanueva, A. Cruz-López, A.A. Zaldívar-Cadena b , A. Tovar-Corona, M.L. Guevara-Romero, and O. Vazquez-Cuchillo, Mat. Sci. in Semiconductor Processing **58** (2017)

8-14.

[12] C.E. Rodríguez-Torres, A.F. Cabrera, L.A. Errico, S. Duhalde, M. Rentería, F. Golmar, and F.H. Sánchez, Physica B **398** (2007) 219-222

[13] Y. Wang, R. Zhang, J. Li, L. Li, and S. Lin, Nanoscale Res. Lett. **9** (2014) 46, (p8).

[14] A. Fakhim Lamrani, M. Ouchri, M. Belaiche, A. El Kenz, M. Loulidi, and A. Benyoussef, Jour. Mag. Mag. Mat. **401** (2016) 977-981.

[15] A. Fakhim Lamrani, M. Ouchri, M. Belaiche, A. El Kenz, M. Loulidi, and A. Benyoussef, Thin Solid Films 570 (2014) 45-48

[16] D. Çakir and O. Gülseren, J. Phys.: C.M. Matter **24** (2012) 305301, (p13).

[17] S. Li, J. Huang, X. Ning, Y. Chen, and Q. Shi, Mater. Res. Express **5** (2018) 045005, (p9).

[18] H. Chen, X. Li, R. Wan, S. Kao-Walter, Y. Lei, and Ch. Leng, Chem. Phys. Letters **695** (2018) 8-18.

[19] W.T. Geng and K. S. Kim, Solid State Communications, **129** (2004) 741-746.

[20] B. J. Nagare, S. Jaware, D. Habale, and S. Chavan, Comp. Mat. Sci. **68** (2013) 127-131

[21] S.-G. Park, B. Magyari-Köpe, and Y. Nishi, Phys. Rev. B 82 (2010) 115109 (9p).

[22] H. Chen, X. Li, R. Wan, S. Kao-Walter, and Y. Lei, Chemical Physics **501** (2018) 60-67.

[23] A. Janotti, J. B. Varley, P. Rinke, N. Umezawa, G. Kresse, and C. G. Van de Walle, Phys. Rev. B 81 (2010) 085212 (7p).

[24] H.-Ch. Wu, S.-H. Li, and S.-W. Lin, Int. Jour. of Photoenergy **2012**, (2012) 823498, (p6).

[25] X. Li, J. Shi, H. Chen, R. Wan, Ch. Leng, S. Chen, and Y. Lei, Comp. Mat. Sci. **129** (2017) 295-303.

[26] F. Aguilera-Granja, A. Vega, and L. C. Balbas, Jour. Chem. Phys. C, 144 (2016) 234312 (8p).

[27] O. Lamiel-Garcia, A. Cuko, M. Calatayud, F. Illas, and Stefan T. Bromley, Nanoscale **9** (2017) 1049-1058.

[28] T. Nishikawa, Y. Shinohara, T. Nakajima, M. Fujita, and S. Mishima, Chem. Letters **28** (1999) 1133-1134.

[29] J.P. Perdew, K. Burke, and M. Ernzerhof, Generalized Gradient Approximation Made Simple, Phys. Rev. Lett. 77 (1996) 3865-3868.

[30] J.M. Soler., E. Artacho, J.D. Gale, A. García, J. Junquera, P. Ordejon, and D. Sánchez-Portal, The SIESTA method for ab initio order-N materials simulation, J. Phys.: Condens. Matter, 14 (2002) 2745-2779.

[31] N. Troullier, and J.L. Martins, Efficient pseudopotentials for plane-wave calculations, Phys. Rev. B, 43 (1991) 1993-2006.

[32] L. Kleinman, and D.M. Bilander, Efficacious Form for Model Pseudopotentials, Phys. Rev. Lett. 48 (1982) 1425-1428.

[33] F. Aguilera-Granja, R. C. Longo, L. J. Gallego, and A. Vega, Jour. Chem. Physics 132 (2010) 184507 (8p).

[34] T. Alonso-Lanza, A. Ayuela, and F. Aguilera-Granja, Phys. Chem. Chem. Phys. 18 (2016) 21913–21920

[35] W. H. Press, S. A. Teukolsky, W. T. Vetterling, and B. P. Flannery, *Numerical Recipes in Fortran*, 2nd edn. (Cambridge University Press, Cambridge, 1992).

TABLE I. Geometrical properties of the system. In column one is the type of impurity and its atomic number (Z) in parenthesis, in colum two the number of oxigen neighbours, in column three the two different Ti-O distances on the edge where the impurity was placed, in colum four the average distance using the twin colums, and finally in column six the deformation parameter as defined in Eq.(3).

Impurity X (Z)	Num. Oxygens Neighbors of X	Distances($\mathring{A}$) Ti-X(1) and Ti-X(2)	Ave. Distance ($\mathring{A}$) Ti-X	Deformation Parameter
2sp				
B (5)	3	2.810, 2.930	2.870	0.871
C (6)	3	2.820, 2.930	2.875	0.871
N (7)	3	2.960, 2.900	2.930	0.870
O (8)	2	2.960, 2.940	2.950	0.846
F (9)	1	3.820, 6.090	4.955	0.644
3sp				
Al (13)	5	2.850, 2.880	2.865	0.969
Si (14)	5	2.790, 2.860	2.825	0.961
P (15)	3	2.730, 3.140	2.935	0.932
S (16)	2	3.120, 2.920	3.020	0.940
Cl (17)	2	3.430, 3.210	3.320	0.830
3d				
Ti (22)	**5**	**2.870, 2.960**	**2.916**	**0.957**
Cr (24)	5	2.830, 2.920	2.875	0.965
Mn (25)	5	2.800, 2.880	2.840	0.972
Fe (26)	4	2.910, 2.900	2.905	0.940
Co (27)	4	2.900, 2.880	2.890	0.941
Ni (28)	5	2.780, 2.850	2.815	0.982
Cu (29)	4	2.920, 2.860	2.890	0.931
4d				
Mo (42)	5	2.980, 3.040	3.010	0.950
Tc (43)	5	2.930, 3.010	2.970	0.966
Ru (44)	5	2.890, 2.980	2.935	0.966
Rh (45)	5	2.900, 2.960	2.930	0.973
Pd (46)	5	2.910, 2.980	2.945	0.985
Ag (47)	4	2.930, 2.990	2.960	0.983
5d				
W (74)	5	2.980, 3.010	2.995	0.952
Re (75)	5	2.940, 3.030	2.985	0.961
Os (76)	5	2.910, 2.990	2.950	0.964
Ir (77)	5	2.740, 3.020	2.880	0.976
Pt (78)	5	2.930, 3.010	2.970	0.983
Au (79)	4	2.950, 3.020	2.985	0.983
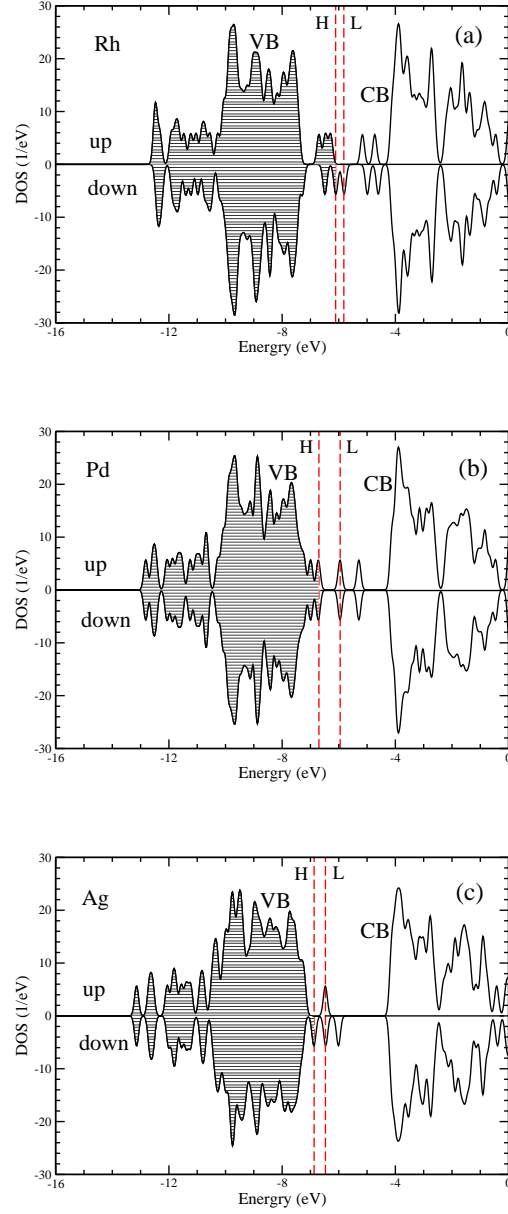
FIG. 13. (Color online) Spin-up and spin-down DOS for Rh (a), Pd (b) and Ag (c), impurities in the Ti_9XO_{20} system (last part of the $4d$ series). The non-monotonous dependence of the impurity levels is clearly shown. Vertical dash lines correspond to the HOMO (H) and LUMO (L) levels. Horizontal lines mark the occupied electronic states. Notice the symmetric DOS for the Pd impurity due to its non-magnetic behavior.